

RESEARCH ARTICLE

10.1002/2016JA022443

Key Points:

- The patch was formed from SED by segmentation associated with a SAPS generated by a substorm
- Antisunward moving patch was halted and evolved in nonclassical way associated with high-latitude reconnection during northward IMF
- Much of patch faded rapidly due to an enhancement of the ionization recombination rate

Supporting Information:

- Supporting Information S1
- Movie S1

Correspondence to:

Q.-H. Zhang,
zhangqinghe@sdu.edu.cn

Citation:

Zhang, Q.-H., et al. (2016), Polar cap patch transportation beyond the classic scenario, *J. Geophys. Res. Space Physics*, 121, 9063–9074, doi:10.1002/2016JA022443.

Received 26 JAN 2016

Accepted 22 AUG 2016

Accepted article online 26 AUG 2016

Published online 20 SEP 2016

Polar cap patch transportation beyond the classic scenario

Qing-He Zhang^{1,2}, Jøran Moen³, Michael Lockwood⁴, Ian McCrea⁵, Bei-Chen Zhang⁶, Kathryn A. McWilliams⁷, Qiu-Gang Zong⁸, Shun-Rong Zhang⁹, J. Michael Ruohoniemi¹⁰, Evan G. Thomas¹⁰, Malcolm W. Dunlop⁵, Rui-Yuan Liu⁶, Hui-Gen Yang⁶, Hong-Qiao Hu⁶, and Mark Lester¹¹

¹Shandong Provincial Key Laboratory of Optical Astronomy and Solar-Terrestrial Environment, Institute of Space Sciences, Shandong University, Weihai, China, ²State Key Laboratory of Space Weather, Chinese Academy of Sciences, Beijing, China, ³Department of Physics, University of Oslo, Oslo, Norway, ⁴Department of Meteorology, University of Reading, Reading, UK, ⁵Space Sciences Division, SSTD, Rutherford Appleton Laboratory, Didcot, UK, ⁶SOA Key Laboratory for Polar Science, Polar Research Institute of China, Shanghai, China, ⁷Institute of Space and Atmospheric Studies, University of Saskatchewan, Saskatoon, Saskatchewan, Canada, ⁸School of Earth and Space Sciences, Peking University, Beijing, China, ⁹MIT Haystack Observatory, Westford, Massachusetts, USA, ¹⁰Bradley Department of Electrical and Computer Engineering, Virginia Tech, Blacksburg, Virginia, USA, ¹¹Department of Physics and Astronomy, University of Leicester, Leicester, UK

Abstract We report the continuous monitoring of a polar cap patch, encompassing its creation, and a subsequent evolution that differs from the classic behavior. The patch was formed from the storm-enhanced density plume, by segmentation associated with a subauroral polarization stream generated by a substorm. Its initial antisunward motion was halted due to a rapidly changing of interplanetary magnetic field (IMF) conditions from strong southward to strong eastward with weaker northward components, and the patch subsequently very slowly evolved behind the duskside of a lobe reverse convection cell in afternoon sectors, associated with high-latitude lobe reconnection, much of it fading rapidly due to an enhancement of the ionization recombination rate. This differs from the classic scenario where polar cap patches are transported across the polar cap along the streamlines of twin-cell convection pattern from day to night. This observation provides us new important insights into patch formation and control by the IMF, which has to be taken into account in *F* region transport models and space weather forecasts.

1. Introduction

Patches of ionization are defined as islands of high-number-density *F* region ionospheric plasma, surrounded by plasma of half the electron concentration or less [Crowley, 1996; Carlson, 2012]. They are formed by ionospheric dynamics in the “cusp region” [Lockwood and Carlson, 1992; Rodger et al., 1994; Moen et al., 2006, 2008; Zhang et al., 2011, 2013a; Valladares et al., 1999], often by processes which segment a preexisting high-density region. The mechanisms that have been suggested to segment the intake of cold solar EUV-ionized plasma into the cusp throat can be divided into three families [Lockwood et al., 2005a; Oksavik et al., 2006; Moen et al., 2006]: (1) interplanetary magnetic field (IMF) regulation of the cusp convection flow pattern, causing alternating intake of high- and low-density plasma [Anderson et al., 1988; Rodger et al., 1994; Milan et al., 2002]; (2) plasma depletion within flow-burst channels due to enhanced recombination, associated with the rapid motion of newly opened magnetic flux tubes [Rodger et al., 1994; Sojka et al., 1993; Valladares et al., 1994; Pitout and Blelly, 2003; Pitout et al., 2004]; and (3) plasma structuring by transient reconnection, where the open-closed boundary (OCB) leaps equatorward to a region of higher-density plasma, followed by poleward relaxation of that boundary, carrying with it the high-density plasma accelerated into the polar flow [Lockwood and Carlson, 1992; Lockwood et al., 2000; Carlson et al., 2006]. Although the third mechanism is now considered to be the dominant one [Lockwood and Carlson, 1992; Carlson, 2012; Zhang et al., 2011, 2013a], it cannot explain all cases (some of which may be caused by a combination of these processes, acting either together or sequentially). Also, a new mechanism involving the substorm cycle has recently been proposed [Zhang et al., 2013b] to help explain the formation of the gaps between patches. In this scenario, bursty sunward return flows, produced by the modulation of nightside reconnection, carry low-density plasma into the cusp region along the dawnside and/or duskside return convection cell, thereby injecting low-density plasma into the convection throat between the patches.

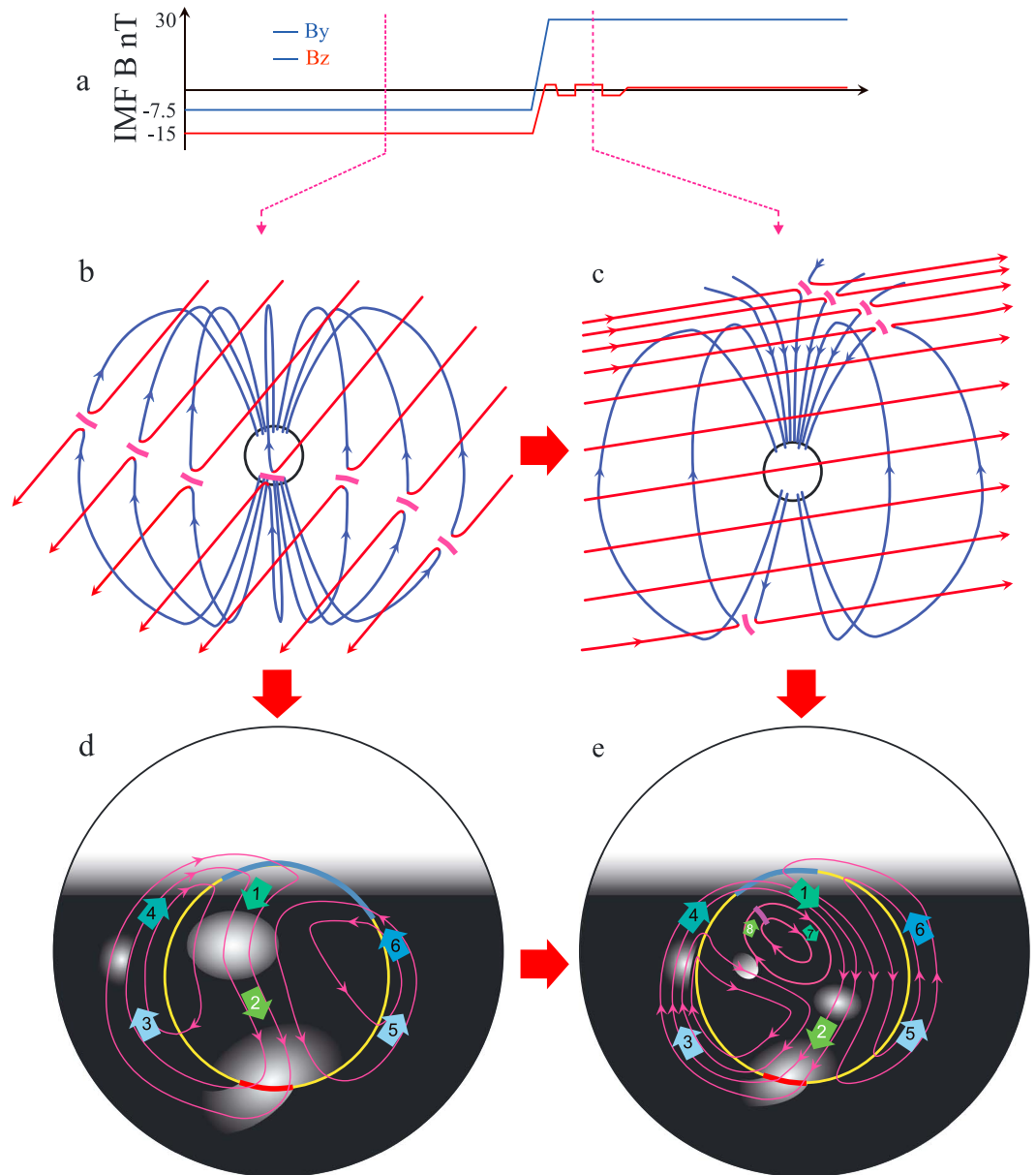


Figure 1. Schematic of the response of the northern polar ionosphere to the IMF turning from strongly southward and weakly downward to strongly duskward, with a weak B_z varying around zero during a substorm recovery phase. Panels shown are (a) the IMF B_y and B_z components, (b and d) the morphology of dayside magnetic reconnection and the polar ionosphere for strong southward and weaker dawnward IMF, (c and e) the morphology of dayside magnetic reconnection and the polar ionosphere for strong duskward and weak northward IMF. In Figures 1b and 1c, the red/blue lines (with arrow) show the magnetic field lines in magnetosheath/magnetosphere and the magenta solid lines show the reconnection X-line at dayside magnetopause. In Figures 1d and 1e, convection streamlines are in mauve. The boundary between open and closed field lines (OCB) lies close to the poleward edge of the auroral oval: the blue/red OCB segments show where magnetic reconnection at the magnetopause/magnetotail is generating/destroying open flux in the Dungey convection cycle [Dungey, 1961; Zhang *et al.*, 2013b, 2015]. The yellow OCB segments are adiabatic (meaning not flowing across) where flow streamlines cross the OCB because it is in motion and the plasma moves with it. The grey scale indicates plasma concentration, with white showing high values generated by solar EUV and black showing low values where plasma has decayed on the nightside.

Generally, patches move across the pole from the dayside to the nightside [Oksavik *et al.*, 2010; Hosokawa *et al.*, 2009], following the flow streamlines of the Dungey convection cycle [Dungey, 1961; Zhang *et al.*, 2013b, 2015]. They have been observed exiting the polar cap and entering the nightside auroral oval, in a manner modulated by the nightside reconnection rate (Figure 1d) [Moen *et al.*, 2007, 2008, 2015; Wood *et al.*,

2009; Zhang *et al.*, 2013b, 2015]. During southward IMF, magnetic reconnection will take place at the dayside low-latitude magnetopause (Figure 1b) and convection then leads to high-density plasma entering the polar cap from subauroral latitudes (arrow 1 in Figure 1d). The resulting patches are transported antisunward across the polar cap (arrow 2) and are termed “blobs” once they exit the polar cap into the nightside auroral oval [e.g., Jin *et al.*, 2014, 2016, and references therein], which is different from the plasma blob in the low-latitude ionosphere [Wang *et al.*, 2015]. These have been seen leaving the polar cap on the nightside, but they can only do so at locations that map to ongoing magnetotail reconnection [Zhang *et al.*, 2013a, 2015; Moen *et al.*, 2007, 2015]. Ionospheric convection can, however, become much more complicated following a sudden change in IMF direction. For example, following a northward turning of the IMF, both dayside low- and high-latitude (lobe) magnetopause reconnection can take place (Figure 1c) [Lockwood and Moen, 1999], leading to the formation of one or two “reverse” convection cells inside the normal convection cell (the case schematically shown in Figure 1e). Interaction with such a reversed convection cell could either accelerate or decelerate the propagation of a patch, perhaps to the point at which the motion of the patch may completely stagnate due to an IMF northward turning [Oksavik *et al.*, 2010; Hosokawa *et al.*, 2011]. It is particularly difficult, however, to study the detailed motion and evolution of patches because of poor data coverage over the poles and the lack of an accurate convection model, able to reproduce the rapid response of ionospheric convection to the sudden change of IMF. In addition, if lobe reconnection takes place of the same field line (simultaneously, or more likely, sequentially) in both hemispheres, then an open field line region is reclosed [Lockwood and Moen, 1999]. This could have two different effects on patch production. If the patch remains in a region where the difference between ion and neutral flow vectors is small, then the loss of plasma will be slow. If, on the other hand, it is exposed to large differences between plasma and neutral velocity it will decay due to enhanced plasma loss rate [Lockwood and Fuller-Rowell, 1987]. In the first case, when the reclosed field line due to dual-lobe reconnection is subsequently opened again for a second time by dayside magnetopause reconnection, it will be reinjected into the polar cap as a new high-number-density patch. In the second case, however, this sequence of reclosing and then opening again would result in low-number-density plasma being injected into the polar cap, which would form a gap between the storm-enhanced density (SED) and the newly formed patch.

Solar extreme ultraviolet radiation (EUV) produces midlatitude ionospheric plasma, which provides a viable reservoir of source plasma for patches, and in some cases densities may be further enhanced by solar wind particles precipitating into the cusp ionosphere [Lockwood *et al.*, 2005b, 2006; Oksavik *et al.*, 2006; Moen *et al.*, 2008; Zhang *et al.*, 2013b, 2015; Goodwin *et al.*, 2015]. During a geomagnetic storm, a ridge of enhanced electron density often occurs in the midlatitude and subauroral region, known as SED [Foster, 1993]. Occasionally, SED extends to higher latitudes driven by subauroral polarization stream (SAPS) electric field, into the cusp and polar cap, where it is termed tongue of ionization (TOI) [Knudsen, 1974; Foster *et al.*, 2005]. This SED/TOI has often been observed to segment into patches [Lockwood and Carlson, 1992; Rodger *et al.*, 1994; Moen *et al.*, 2008; Zhang *et al.*, 2011, 2013a, 2015; Valladares *et al.*, 1999]. It is important to understand and predict the occurrence of patches for space weather forecasting purposes, because steep density gradients at patch boundaries with multiple small-scale structures can give large bearing errors in HF over-the-horizon radars and phase and amplitude scintillation in transionospheric radio signals, including ground-to-satellite communications and other navigation applications [Crowley *et al.*, 2000; Zou *et al.*, 2013]. Such predictions will require understanding of how patches are likely to evolve in response to given variations in interplanetary conditions combined with “nowcasting” observations of the spatial distribution of ionospheric densities in the polar cap. Here we present continuous monitoring of both the total electron content (TEC, the integral with height of the electron concentration, 1 TEC unit = 10^{16} el/m²) and flow over a large fraction of the Northern Hemisphere convection zone (with time resolution of 5 min) by combining TEC from a dense and extensive array of GPS receivers [Coster *et al.*, 2003; Stolle *et al.*, 2006] with the large-scale coverage of the convection flows (averaging in 5 min) provided by the Super Dual Auroral Radar Network (SuperDARN) radars [Chisham *et al.*, 2007] using the map potential technique [Ruohoniemi and Baker, 1998; Thomas *et al.*, 2013], together with measurements from the Special Sensors-Ions, Electrons, and Scintillation thermal plasma analysis package on board the Defense Meteorological Satellite Program (DMSP) F18 satellite [Hardy *et al.*, 1984] and observations from the Poker Flat Incoherent Scatter Radar (PFISR) [Nicolls and Heinselman, 2007]. We demonstrate that a stirred lobe cell in the dusk sector due to IMF B_z positive prevents a newly separated patch from being transported across the polar cap.

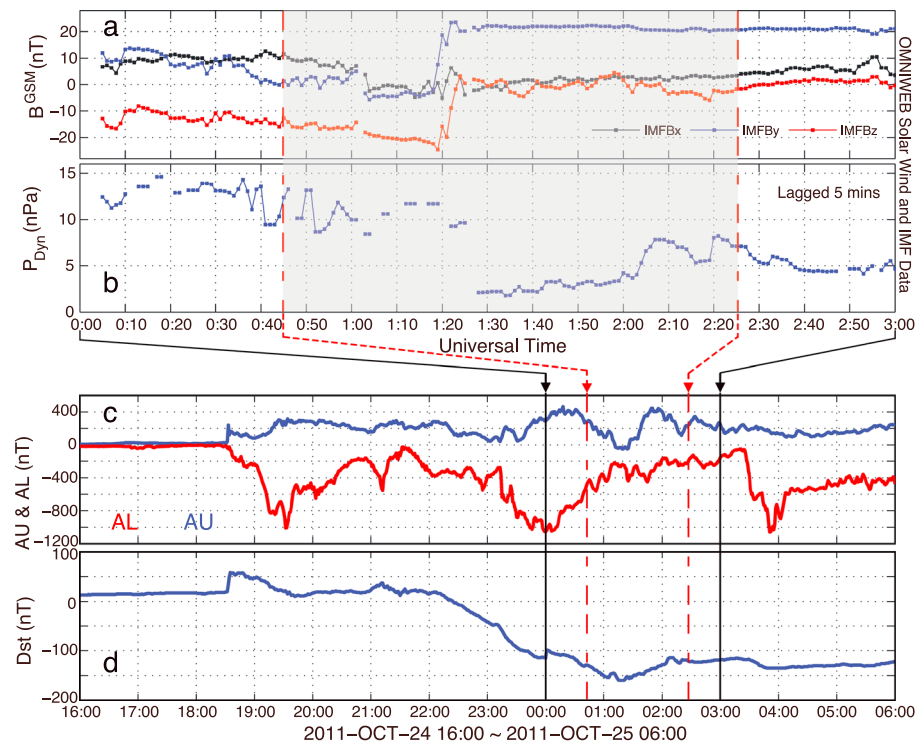


Figure 2. An overview of the interplanetary conditions, the auroral electrojet indices, and the *Dst* index on 25 October 2011. Parameters shown are (a) the IMF components in GSM coordinates; (b) the solar wind dynamic pressure, P_{Dyn} ; (c) the provisional AE auroral electrojet geomagnetic indices from 11 stations: the blue line is AU (auroral upper) and the red line is AL (auroral lower); and (d) the *Dst* index. Interplanetary data have been lagged to the nose of bow shock by OMNIWeb (based on the measurements from Wind satellite) and then shifted 5 min to the magnetosphere. The shading area highlighted the interval of interest.

2. Observations and Results

On 24 October 2011, a coronal mass ejection (CME) impacted the magnetopause at 18:40 UT, giving an enhancement of solar wind dynamic pressure, P_{Dyn} , and resulting in an intense geomagnetic storm (*Dst*, minimum of -160 nT) [Zou *et al.*, 2013]. One day later, at about 01:25 UT, a reverse shock (sudden decrease in P_{Dyn} due to a rapid reduction in solar wind number density) impacted the magnetosphere with a sudden turning of IMF to a strongly duskward and weakly northward direction (Figures 2a and 2b). Ahead of the reverse shock (Figure 2b), the IMF at Earth was large and variable, containing an interval of exceptionally strong southward field (B_z ; Figure 2a, red), during which a global response of the convection pattern would be expected [Morley and Lockwood, 2006]. Owing to the sudden duskward and northward turning of the IMF and the sudden decrease of P_{Dyn} at about 01:20 UT (Figure 2a), however, the expected global response becomes more complex [Greenwald *et al.*, 1990; Chisham *et al.*, 2000]. During the storm, there were three substorm onsets, at 19:00, 23:13, and 03:26 UT, shown by the AL (auroral lower) index falling to -1000 nT (Figure 2c). These substorms would have been associated with magnetic reconnection in the cross tail current sheet [Cowley and Lockwood, 1992], as well as producing SAPS, characterized by low-density plasma connecting via flow bursts from the nightside to the dayside, along the duskside streamlines of the convection cell [Foster and Burke, 2002; Wang and Lühr, 2011; Hosokawa *et al.*, 2010].

Figure 3 reveals the formation and evolution of a patch, together with the mapping of the TEC and flow streamlines from the SuperDARN radar (Movie S1 in the supporting information) [Thomas *et al.*, 2013; Zhang *et al.*, 2013b, 2015]. Streamlines and vectors of the ionospheric flows derived from the Northern Hemispheric SuperDARN velocity measurements shown on geomagnetic/magnetic local time (MLT) grids, obtained from the “map potential” algorithm [Ruohoniemi and Baker, 1998]. The grayed concentric circles indicate lines of constant magnetic latitude in 10° increments. Noon is located at the top of each pattern. The dotted line across each panel is the day-night terminator at 100 km altitude. The blue circles highlight

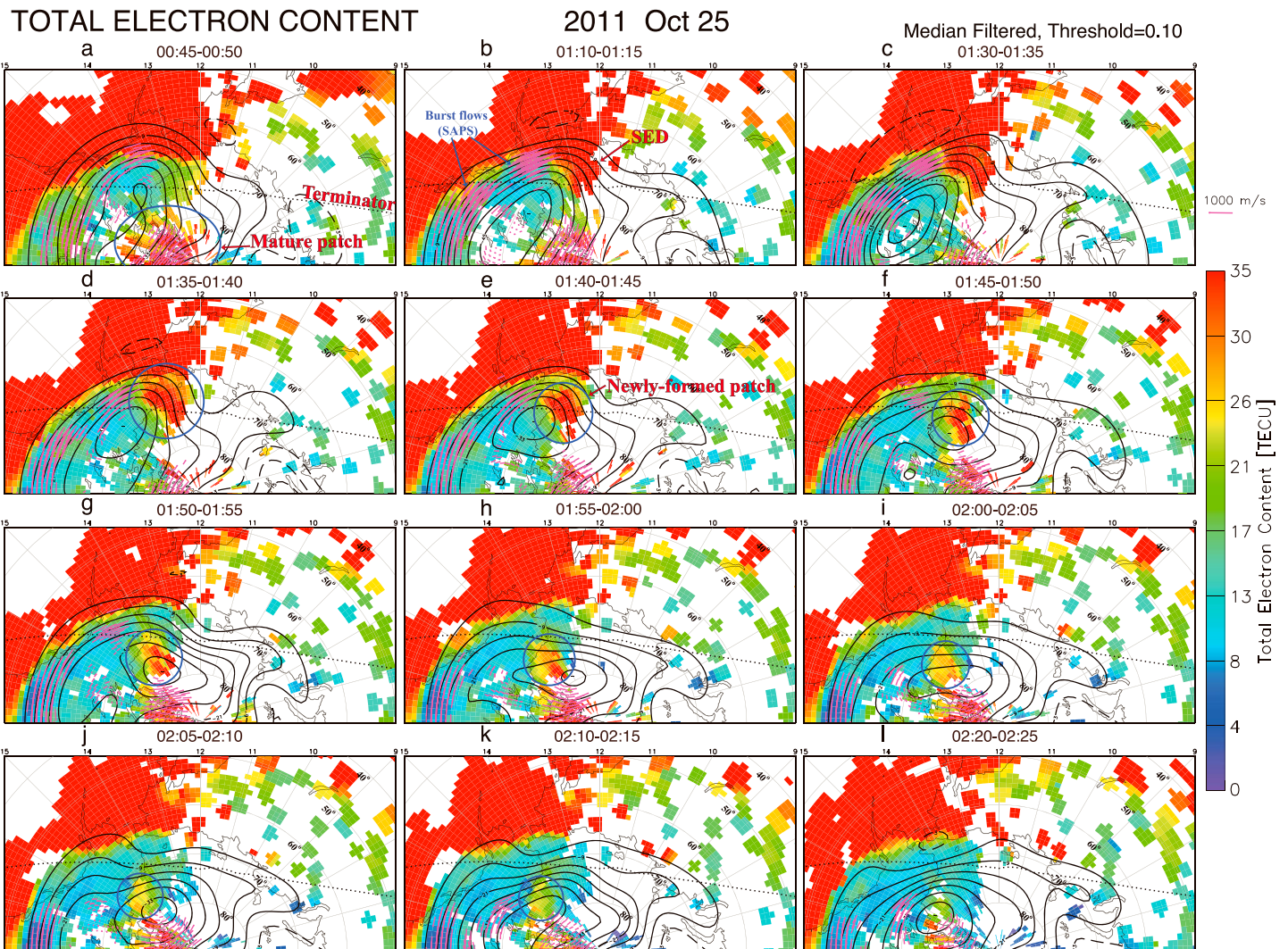


Figure 3. Extracts from a full series of 2-D maps of median-filtered TEC and ionospheric convection on a geomagnetic latitude/MLT grid for the dayside sectors with noon at the top (Movie S1). Streamlines and drift velocity vectors of ionospheric convection obtained from the map potential algorithm at the location of SuperDARN actual radar measurements in the Northern Hemisphere. The dotted line across each panel is the day-night terminator at 100 km altitude. The blue circles highlight the polar cap patch, the evolution of which is followed here.

the polar cap patch, the evolution of which is followed here. Note that at locations where there are no radar echoes, the potentials are derived by using a model flow pattern determined by the prevailing IMF orientation and fitted to the observations that are available. For this event, the total number of GPS receiver sites is likely 4000–6000, with ~270 receivers with geographic latitude of > 60°N. The distribution of the receiver sites is similar to that in the GPS TEC data shown in Figure 3, with descent coverage in Greenland, Northern Alaska, Northern Europe, and Canada.

In Figure 3a, a normal TEC distribution for the daytime sectors exists in the northern hemisphere, with a mature polar cap patch deeply embedded in the polar cap (highlighted by the blue semiellipse in Figure 3a). As time advances, a clear SED plume begins to enter the polar cap region in the afternoon sector (seen in Figure 3b), while a clear region of low-density plasma, poleward of 60°, also convects toward the cusp “throat” (around 70° latitude near 12:00 MLT) and encounters the SED plume at subauroral latitudes (around 65° and 14:00 MLT in Figures 3b and 3c). A rapid burst of sunward return flow is observed to evolve from the nightside toward the dayside (see the drift vector lower latitude at the afternoon and dusk sectors in Figures 3b–3g and Movie S1) developing into a SAPS event [Zou *et al.*, 2013], which serves to transport low-density plasma into place behind the regions of high-density plasma pinching off from the SED. This causes the leading part of the SED plume to

begin segmenting into a patch at about 01:35 UT. The patch is completely separated from the SED (the high dayside TEC values) by about 01:40 UT (highlighted by the blue circle in Figure 3e). After its formation, however, the patch does not evolve in the classic scenario to move along the streamlines of the twin-cell convection patterns. Rather, it slowly moves northeastward (anticlockwise direction), stagnates, and moves slowly toward dusk, while it rapidly fades (reduces in intensity) during its evolution (Figures 3f–3k). The lifetime of this patch is about 40 min, which is much shorter than the 2–3 h patch lifetimes predicted and observed in previous studies [Lockwood and Carlson, 1992; Crowley, 1996; Moen *et al.*, 2006; Carlson, 2012; Zhang *et al.*, 2011, 2013b, 2015]. We will discuss the mechanisms responsible for the formation and somewhat unusual evolution of this patch in the next section.

3. Discussion

3.1. Formation Mechanisms of the Patch

We note that the IMF suddenly turned strongly duskward (IMF B_y positive) and weakly northward (IMF B_z positive) before the reverse shock arrived at about 01:25 UT. After this, it remained strongly duskward with north-southward variations (B_z) around zero (Figure 2a). This sudden duskward turning would be expected to lead to a dawnward expansion of the afternoon convection cell after a certain time delay [Greenwald *et al.*, 1990; Chisham *et al.*, 2000], as demonstrated by the observations from the SuperDARN radars (Figure 3f). This type of response is consistent with the results from previous studies [Greenwald *et al.*, 1990; Chisham *et al.*, 2000]. The formation of the patch in our observations took place prior to this expansion, indicating that the sudden duskward turning did not cause an immediate segmentation of the patch but subsequently contributed to its evolution.

The Poker Flat Incoherent Scatter Radar (PFISR) was operated in an International Polar Year four-beam mode during the interval 24–25 October 2011 [Sojka *et al.*, 2009; Zou *et al.*, 2013]. PFISR is located near Fairbanks, Alaska, which was at a subauroral latitude, near the duskside edge of the SED seen in Figures 3b–3d, during the interval of interest (Figure 4a). PFISR data therefore offer us a good opportunity to monitor the time evolution of the altitude profile of the corresponding ionospheric plasma, which will be very helpful for discussing the formation mechanism of the patch segmented from the SED seen in Figure 3d. The observations from PFISR beam 2 (magnetic field-aligned beam) show that there was pulsed particle precipitation characterized by electron density and electron temperature enhancement before about 01:55 UT and even during the period of the encounter with SED-like plasma before 01:00 UT (Figures 5a and 5b), suggesting an association with pulsed dayside magnetopause reconnection. During this period of particle precipitation, the ion temperature also increased (Figure 5c), showing an increase in flow speed. This region of increased flow can be identified as corresponding to the SAPS seen in Figure 3. Beam 4 of PFISR, which was looking toward the region of low plasma density, also observed the Ti enhancement at lower latitudes (Figures 5e and 5g), again consistent with the SAPS flow observed by the SuperDARN radars. The fact that the plasma patch formed during the interval between periods of Ti enhancement around 01:10 and 01:40 UT, seen both by beams 2 and 4, suggests that the patch formation was associated both with the dayside reconnection and with the SAPS. After 01:55 UT, both beams 2 and 4 observed the low-density features, which are consistent with the observations from GPS TEC (Figures 3e–3i).

Based on the GPS TEC, SuperDARN, and PFISR observations, we propose that the patch formation mechanism was as follows. With the onset of rapid dayside reconnection, the open-closed field line boundary (OCFLB) would be expected to leap equatorward, resulting in an electric field configuration which allowed the SAPS to encounter the SED [Lockwood and Carlson, 1992; Zhang *et al.*, 2011, 2013a]. As a result of this encounter, the SED seems to be “cut” and the leading part of the SED plume was segmented into a patch (ringed in blue) with a gap of low-density plasma from nightside being entrained in the burst flow. The patch initially moved poleward, due to the poleward relaxation of the OCFLB and the low-density plasma carried by the SAPS (Figures 3b–3g and Figure 6). In summary, the SAPS with low-density plasma, associated with the 23:13 UT substorm (Figure 2c), together with local expansion and contraction of the OCFLB, played the key role in forming the patch segmented from the leading part of the SED plume.

3.2. Evolution of the Patch

The subsequent evolution of the patch is more complicated than that in the classic scenario where expected that the patches drift transpolar in a Dungey twin-cell convection pattern [Lockwood and Carlson, 1992;

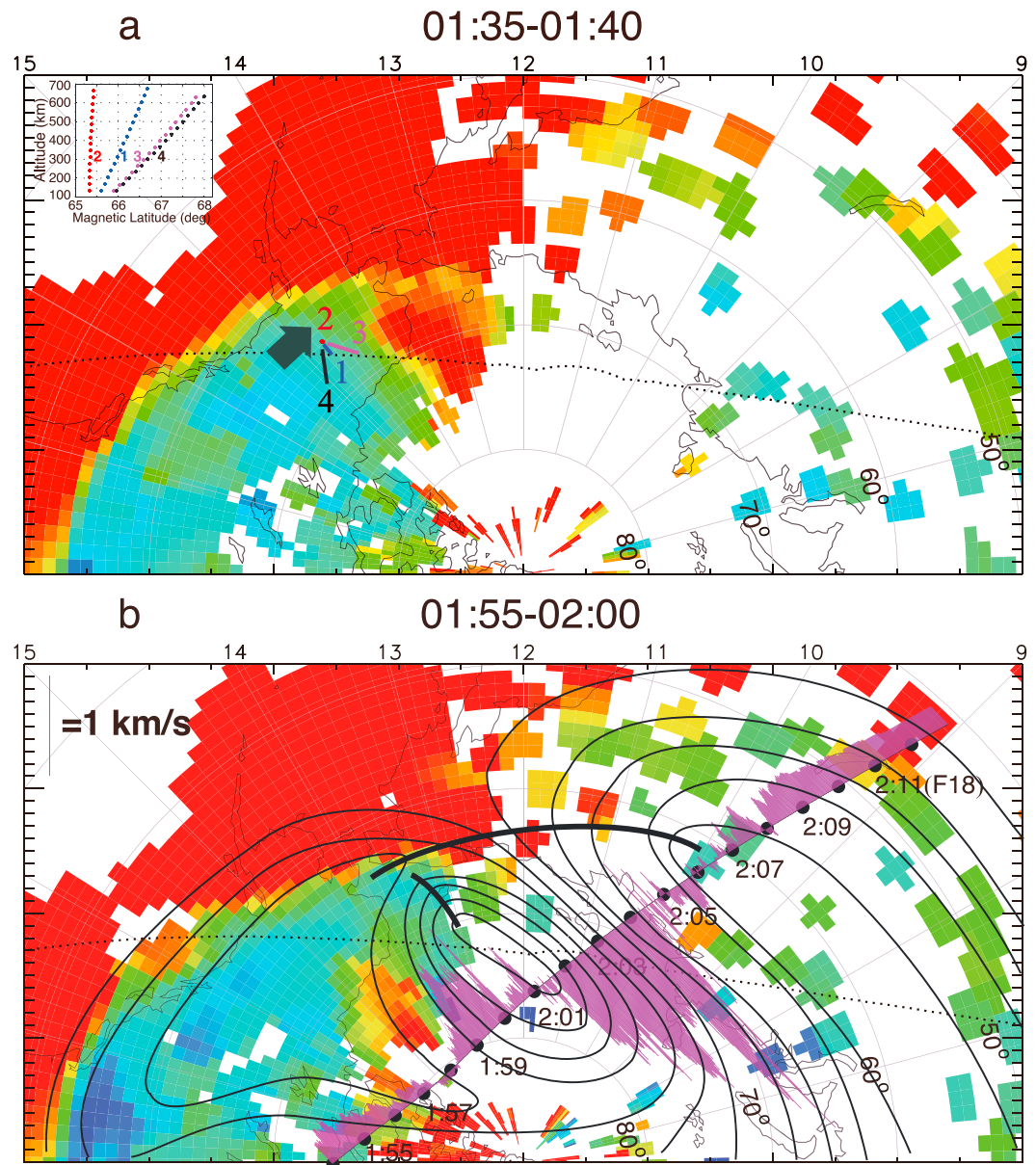


Figure 4. The lines of sight of the four beams of Poker Flat Incoherent Scatter Radar and the schematic convection pattern observed by DMSP F18 projected into the TEC map. The PFISR beam configuration as a function of altitude and magnetic latitude is shown in the top left corner of Figure 4a, where beam 1 is pointing toward magnetic north (geographically vertical), beam 2 is located at the lowest latitude roughly pointing along the local magnetic field line, and beams 3 and 4 are looking northwestward and northeastward, respectively. The flows in Figure 4b are schematic drawn to a set of rules but they are not unique solutions. The potential distribution along the DMSP F18 pass was computed from the cross-track velocity assuming that the pattern did not change over the duration of the pass. Streamlines were then drawn to join up points of equal potential along the pass. Away from the satellite pass the forms of the streamlines were constructed to be consistent with both the prevailing IMF orientation and with the matched potential plots from the SuperDARN radars in those areas where echoes were received. The thick black solid lines on the convection pattern show the reconnection X-line at high- and low-latitude magnetopause.

Carlson, 2012; Moen *et al.*, 2006; Zhang *et al.*, 2011, 2013b, 2015]. As illustrated in Figure 4b, the patch is situated duskward of the stirred lobe cell, in a region of slow convection. It appears that the lobe cell stirs low-density plasma and the patch has stagnated in a region of weak flow.

The SuperDARN convection maps are based on a combination of the available measurements and statistical convection model organized by IMF configurations [Ruohoniemi and Baker, 1998]. It is better to compare the

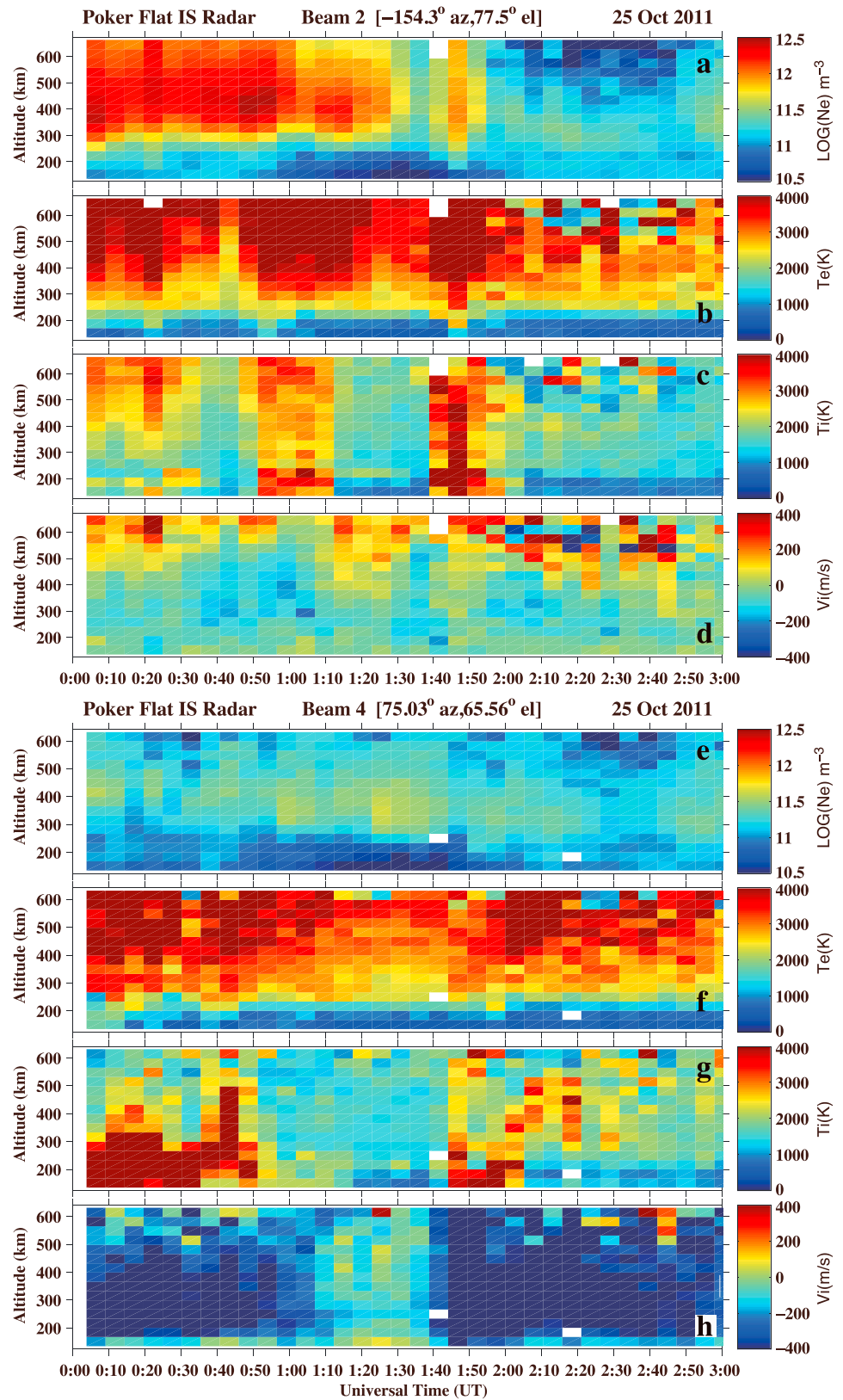


Figure 5. Plasma parameters observed by beam 2 (field-aligned) and beam 4 (northeast looking) of PFISR on 25 October 2011. Parameters from top to bottom are (a and e) electron density (N_e), (b and f) electron temperature (T_e), (c and g) ion temperature (T_i), and (d and h) line-of-sight velocity (V_i , positive away from the radar) as a function of time and altitude.

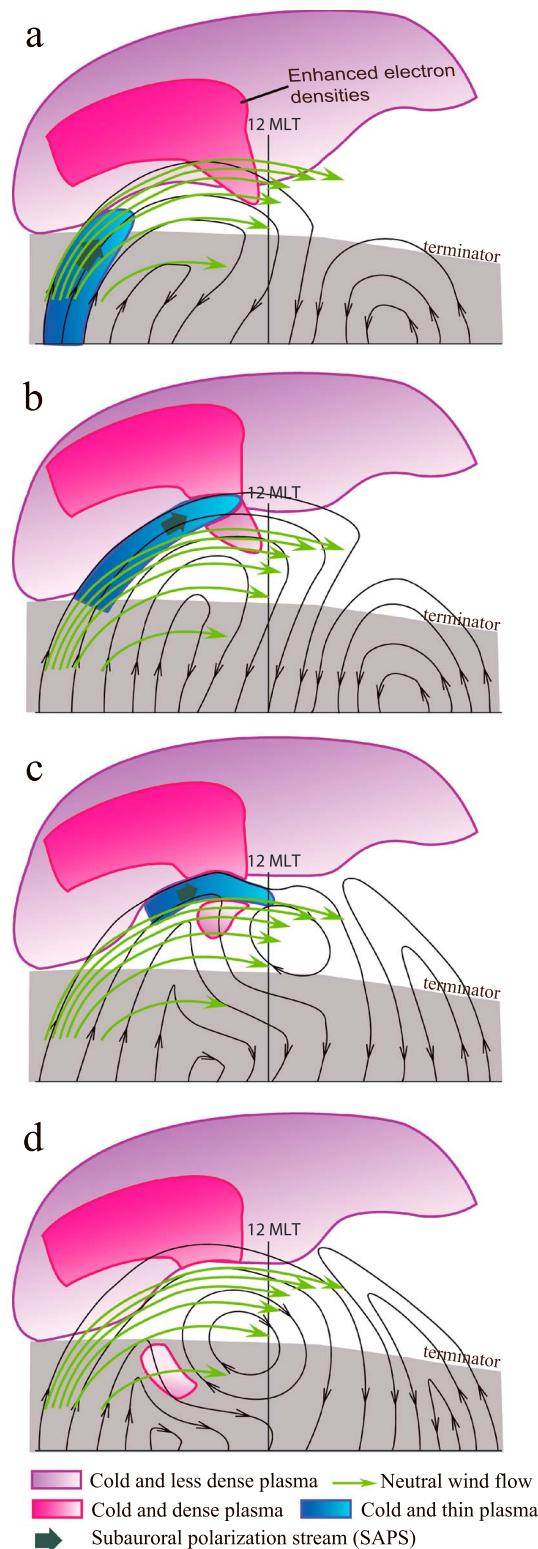


Figure 6. Schematic of the formation and evolution of the polar cap patch. The color shaded regions show the plasma regions from different sources. The series of diagrams show how a SED is segmented into patches by the SAPS associated with a substorm and how the patch evolves associated with the high-latitude lobe reconnection during the IMF northward turning.

in situ ion drift velocity measurements from the DMSP F18 satellite for the convection, where the SuperDARN data are sparse. This is the case around and westward of the patch throughout this period, and so the statistical convection model is filling this data gap [Ruohoniemi and Baker, 1998]. The DMSP F18 satellite measures the cross-orbit track component of the flow, which can be used to calculate the potential along the track and constrain the equipotential flow streamlines in the polar ionosphere (Figure 4b). These data showed a reverse cell inside the afternoon convection cell around the patch (see the superposed vectors in Figures 4b and 3h). This reverse cell will have been generated by high-latitude lobe reconnection during the strong duskward and weak northward IMF conditions. These conditions would be expected to lead to dayside reconnection simultaneously occurring at the low- and high-latitude (lobe) magnetopause (schematically shown in Figure 1c) [Lockwood and Moen, 1999], leading to the localized sunward expansion and the reverse cell seen in DMSP observations. The motion of the patch is consistent with the flows seen by DMSP F18, and we conclude that most of the difference between the patch motion and the SuperDARN flow equipotential is because the model-based extrapolation of the convection may be misleading in this area. Note that around 01:58 UT, DMSP F18 briefly observed slow downward flow. This is between the inflow to the lobe reconnection site and where flows are associated with the equatorward expansion of the dusk “adiarctic” polar cap boundary (meaning “not flowing across”). We interpret this as an effect of ongoing reconnection in the low-latitude magnetopause, as shown in Figure 4b. During its evolution duskward of the reverse cell, the patch rapidly faded (within about 40 min). This short lifetime of the patch is most likely to be

caused by the effect of the opposite ion drift and neutral wind directions leading to enhanced frictional ion heating and thus faster plasma recombination. Even though there are no direct observations of the neutral wind available, it is reasonable to expect that the changes in the ion flow only slowly influence the neutral winds because the neutral atoms are so much more numerous than the ions. Simulations from ionosphere-thermosphere models show that a strong neutral wind is established in the afternoon auroral oval and this persists in a dawnward direction into the cusp region [Lockwood and Fuller-Rowell, 1987; Farmer *et al.*, 1988]. Thus, the patch that has been entrained duskward of the lobe circulation cell and is moving toward dusk is expected to have an ion velocity vector that makes a large angle with the neutral wind vector and the square of the vector difference between the two, which is associated with frictional heating [Lockwood and Fuller-Rowell, 1987; Farmer *et al.*, 1988], would be large. This means that the ion heating is greatly enhanced as is the plasma loss rate [Schunk *et al.*, 1975]. The O^+ lifetime (reciprocal of the recombination rate) in the polar region at 275 km altitude is estimated at ~ 50 min in October, while an elevation of ion temperature by 750 K, due to frictional heating by an ion-neutral relative velocity of ~ 1000 m/s, can lead to ~ 30 min lifetime.

The interval covered by Figures 3a and 3b is the recovery phase of the second substorm, as indicated by *AU* and *AL* indices (Figure 2d), after which the SAPS evolved from duskside to dayside in the afternoon sector, as seen by the SuperDARN radars (Figures 3a–3c). The SAPS transported low-density plasma toward the dayside, where the low-density plasma produced the gap between the patch and the SED, as schematically illustrated in Figures 6a–6c. Thus, SAPS associated with a substorm, together with the local expansion and contraction of OCFLB, has played a key role in forming the gap between the patch and the rest part of the SED. This can explain why such gaps are larger if substorm activity is absent [Wood *et al.*, 2009; Zhang *et al.*, 2013b, 2015] and why patches can be segmented even before they enter the cusp region [Moen *et al.*, 2006]. After forming in the subauroral region, the patch moved slowly northeastward and stagnated duskward of a reverse cell in afternoon sectors with a fast fading. Part of this may be because the plasma in sunward edge of the patch will recombine much faster than that in the antisunward edge (schematically shown in Figure 6), giving the patch, as seen in plasma concentrations, an apparent antisunward motion due to the strong dawnward neutral wind established in the afternoon sector auroral oval be strongest in the cusp region and gets weaker as one going antisunward of the cusp [Lockwood and Fuller-Rowell, 1987].

The apparently anomalous motion seems to be due to localized sunward expansion and the formation of a new reverse cell inside of the afternoon convection cell, generated by the dayside low- and high-latitude (lobe) magnetopause reconnection [Lockwood and Moen, 1999], respectively. This reverse cell was detected by DMSP F18. During its formation, the neutral wind would not have had time to respond to the sudden IMF change but would have maintained its previous velocity toward the cusp region from the duskside (shown schematically by the green flow lines in Figure 6), resulting in enhanced ion-neutral vector velocity difference and ion temperature [Lockwood and Fuller-Rowell, 1987; Farmer *et al.*, 1988], leading to enhanced plasma loss rate [Lockwood and Fuller-Rowell, 1987]. Hence, this patch faded more rapidly than those which continue to move toward the nightside. Note that the neutral wind effect will tend to make northern hemisphere patches that formed during southward IMF and are subsequently moved toward dawn by a positive B_y more long-lived than those moved toward dusk by negative B_y .

4. Conclusions

The observations presented here have recorded for the first time the context of the evolution of a newly formed polar cap patch that stagnated in the polar cap dusk sector. In this instance, the SAPS associated with a substorm, together with the local expansion and contraction of the OCFLB, helped to form the gap between the patch and the SED. After formation, the patch was entrained in a lobe cell that was established as a result of the changes in the IMF orientation stimulating lobe reconnection. The rapid fading in number density was probably due to the enhanced recombination rate associated with the divergence of the flow direction between the neutral wind and the plasma convections in the newly formed reverse cell. This scenario challenges the simplistic picture that all plasma patches formed in the dayside inflow region will subsequently move across the polar cap and exit at night [Carlson, 2012; Zhang *et al.*, 2013b, 2015] and is to be considered when improving space weather forecasts of polar cap patch related phenomena.

Acknowledgments

This work in China was supported by the National Basic Research Program (grant 2012CB825603), the National Natural Science Foundation (grants 41574138, 41274149, and 41274148), the Shandong Provincial Natural Science Foundation (grant JQ201412), the International Collaboration Supporting Project, Chinese Arctic and Antarctic Administration (IC201511), the Chinese Meridian Project, and the Specialized Research Fund for State Key Laboratories. J. Moen is supported by the Research Council of Norway grant 230996. The work at Reading University was supported by STFC consolidated grant ST/M000885/1. SuperDARN is a collection of radars funded by national scientific funding agencies in Australia, Canada, China, France, Japan, South Africa, United Kingdom, and United States of America. The Virginia Tech authors acknowledge the support of NSF awards AGS-0946900 and AGS-0838219 and a graduate research fellowship from the Virginia Space Grant Consortium. M. Lester acknowledges support from STFC grant ST/K001000/1 and NERC grant NE/K011766/1. The GPS TEC acquisition effort is led by A.J. Coster at MIT Haystack Observatory. The GPS TEC and SuperDARN data are available on the public database: <http://vt.superdarn.org/tiki-index.php?page=DaViT+TEC>. We also thank the NOAA FTP for making available the DMSP data (ftp://ftp.ngdc.noaa.gov/STP/satellite_data/), the NASA OMNIWeb for the solar wind, the Madrigal database for the Poker Flat incoherent radar data (<http://madrigal.haystack.mit.edu/madrigal/>), IMF (http://omniweb.gsfc.nasa.gov/html/sc_merge_data1.html) and WDC C1, and Kyoto for the AE indices (<http://wdc.kugi.kyoto-u.ac.jp/wdc/Sec3.html>).

References

- Anderson, D., J. Buchau, and R. Heelis (1988), Origin of density enhancements in the winter polar cap ionosphere, *Radio Sci.*, *23*, 513–519.
- Carlson, H. C. (2012), Sharpening our thinking about polar cap ionospheric patch morphology, research, and mitigation techniques, *Radio Sci.*, *47*, RS0L21, doi:10.1029/2011RS004946.
- Carlson, H. C., J. Moen, K. Oksavik, C. P. Nielsen, I. W. McCrea, T. R. Pedersen, and P. Gallop (2006), Direct observations of injection events of subauroral plasma into the polar cap, *Geophys. Res. Lett.*, *33*, L05103, doi:10.1029/2005GL025230.
- Chisham, G., M. Pinnock, A. S. Rodger, and J.-P. Villain (2000), High-time resolution conjugate SuperDARN radar observations of the dayside convection response to changes in IMF By, *Ann. Geophys.*, *18*, 191–201.
- Chisham, G., et al. (2007), A decade of the Super Dual Auroral Radar Network (SuperDARN): Scientific achievements, new techniques and future directions, *Surv. Geophys.*, *28*, 33–109, doi:10.1007/s10712-007-9017-8.
- Coster, A. J., J. C. Foster, and P. J. Erickson (2003), Monitoring the ionosphere with GPS, *GPS World*, *14*(5), 42–45.
- Cowley, S. W. H., and M. Lockwood (1992), Excitation and decay of solar-wind driven flows in the magnetosphere-ionosphere system, *Ann. Geophys.*, *10*, 103–115.
- Crowley, G. (1996), Critical review of ionospheric patches and blobs, in *Review of Radio Science 1992–1996*, edited by W. R. Stone, pp. 619–648, Oxford Univ. Press, U. K.
- Crowley, G., A. J. Ridley, D. Deist, S. Wing, D. J. Knipp, B. A. Emery, J. Foster, R. Heelis, M. Hairston, and B. W. Reinisch (2000), Transformation of high-latitude ionospheric F region patches into blobs during the March 21, 1990, storm, *J. Geophys. Res.*, *105*, 5215–5230.
- Dungey, J. W. (1961), Interplanetary magnetic field and the auroral zones, *Phys. Rev. Lett.*, *6*, 47–48.
- Farmer, A. D., M. Lockwood, T. J. Fuller-Rowell, K. Suvanto, and U. P. Lovhaug (1988), Model predictions of the occurrence of non-Maxwellian plasmas, and analysis of their effects on EISCAT data, *J. Atmos. Terr. Phys.*, *50*, 487–499.
- Foster, J. C. (1993), Storm time plasma transport at middle and high latitudes, *J. Geophys. Res.*, *98*, 1675–1689.
- Foster, J. C., and W. J. Burke (2002), SAPS: A new characterization for sub-auroral electric fields, *Eos Trans. AGU*, *83*, 393–394.
- Foster, J. C., et al. (2005), Multiradar observations of the polar tongue of ionization, *J. Geophys. Res.*, *110*, A09S31, doi:10.1029/2004JA010928.
- Goodwin, L., et al. (2015), Swarm in situ observations of F-region polar cap patches created by cusp precipitation, *Geophys. Res. Lett.*, *42*, 996–1003, doi:10.1002/2014GL062610.
- Greenwald, R. A., K. B. Baker, J. M. Ruohoniemi, J. R. Dudeney, M. Pinnock, N. Mattin, J. M. Leonard, and R. P. Lepping (1990), Simultaneous conjugate observations of dynamic variations in high-latitude dayside convection due to changes in IMF By, *J. Geophys. Res.*, *95*, 8057–8072.
- Hardy, D. A., L. K. Schmitt, M. S. Gussenhoven, F. J. Marshall, and H. C. Yeh (1984), Precipitating electron and ion detectors (SSJ/4) for the block 5D/flights 6-10 DMSP (Defense Meteorological Satellite Program) satellites: Calibration and data presentation, Rep. AFGL-TR-84-0317, Air Force Geophys. Lab., Hanscom Air Force Base, Ass.
- Hosokawa, K., T. Kashimoto, S. Suzuki, K. Shiokawa, Y. Otsuka, and T. Ogawa (2009), Motion of polar cap patches: A statistical study with all-sky airglow imager at Resolute Bay, Canada, *J. Geophys. Res.*, *114*, A04318, doi:10.1029/2008JA014020.
- Hosokawa, K., T. Tsugawa, K. Shiokawa, Y. Otsuka, N. Nishitani, T. Ogawa, and M. R. Hairston (2010), Dynamic temporal evolution of polar cap tongue of ionization during magnetic storm, *J. Geophys. Res.*, *115*, A12333, doi:10.1029/2010JA015848.
- Hosokawa, K., J. I. Moen, K. Shiokawa, and Y. Otsuka (2011), Decay of polar cap patch, *J. Geophys. Res.*, *116*, A05306, doi:10.1029/2010JA016297.
- Jin, Y., J. I. Moen, and W. J. Miloch (2014), GPS scintillation effects associated with polar cap patches and substorm auroral activity: Direct comparison, *J. Space Weather Space*, *4*, doi:10.1051/swsc/2014019.
- Jin, Y., J. I. Moen, W. J. Miloch, L. B. N. Clausen, and K. Oksavik (2016), Statistical study of the GNSS phase scintillation associated with two types of auroral blobs, *J. Geophys. Res. Space Physics*, *121*, 4679–4597, doi:10.1002/2016JA022613.
- Knudsen, W. C. (1974), Magnetospheric convection and the high-latitude F2 ionosphere, *J. Geophys. Res.*, *79*, 1046–1055.
- Lockwood, M., and H. C. Carlson (1992), Production of polar cap electron density patches by transient magnetopause reconnection, *Geophys. Res. Lett.*, *19*, 1731–1734.
- Lockwood, M., and J. Moen (1999), Reconfiguration and closure of lobe flux by reconnection during northward IMF: Evidence for signatures in cusp/cleft auroral emissions, *Ann. Geophys.*, *17*, 996–1011.
- Lockwood, M., and T. J. Fuller-Rowell (1987), The modelled occurrence of non-thermal plasma in the ionospheric F-region and possible consequences for ion outflows into the magnetosphere, *Geophys. Res. Lett.*, *14*, 371–374.
- Lockwood, M., I. W. McCrea, S. E. Milan, J. Moen, J. C. Cerisier, and A. Thorolfsson (2000), Plasma structure within poleward-moving cusp-cleft auroral transients: EISCAT Svalbard radar observations and an explanation in terms of large local time extent of events, *Ann. Geophys.*, *18*, 1027–1042.
- Lockwood, M., J. A. Davies, J. Moen, A. P. van Eyken, K. Oksavik, I. W. McCrea, and M. Lester (2005a), Motion of the dayside polar cap boundary during substorm cycles: II. Generation of poleward-moving events and polar cap patches by pulses in the magnetopause reconnection rate, *Ann. Geophys.*, *23*, 3513–3532.
- Lockwood, M., J. Moen, A. P. van Eyken, J. A. Davies, K. Oksavik, and I. W. McCrea (2005b), Motion of the dayside polar cap boundary during substorm cycles: I. Observations of pulses in the magnetopause reconnection rate, *Ann. Geophys.*, *23*, 3495–3511.
- Lockwood, M., B. S. Lanchester, S. K. Morley, K. Throp, S. E. Milan, M. Lester, and H. U. Frey (2006), Modeling the observed proton aurora and ionospheric convection responses to changes in the IMF clock angle: 2. Persistence of ionospheric convection, *J. Geophys. Res.*, *111*, A02306, doi:10.1029/2003JA010307.
- Milan, S. E., M. Lester, and T. K. Yeoman (2002), HF radar polar patch formation revisited: Summer and winter variations in dayside plasma structuring, *Ann. Geophys.*, *20*(4), 487–499.
- Moen, J., H. C. Carlson, K. Oksavik, C. P. Nielsen, S. E. Pryse, H. R. Middleton, I. W. McCrea, and P. Gallop (2006), EISCAT observations of plasma patches at sub-auroral cusp latitudes, *Ann. Geophys.*, *24*, 2363–2374.
- Moen, J., N. Gulbrandsen, D. A. Lorentzen, and H. C. Carlson (2007), On the MLT distribution of F-region polar cap patches at night, *Geophys. Res. Lett.*, *34*, L14113, doi:10.1029/2007GL029632.
- Moen, J., X. C. Qiu, H. C. Carlson, R. Fujii, and I. W. McCrea (2008), On the diurnal variability in F2-region plasma density above the EISCAT Svalbard radar, *Ann. Geophys.*, *26*, 2427–2433.
- Moen, J., K. Hosokawa, N. Gulbrandsen, and L. B. N. Clausen (2015), On the symmetry of ionospheric polar cap patch exits around magnetic midnight, *J. Geophys. Res. Space Physics*, *120*, 7785–7797, doi:10.1002/2014JA020914.
- Morley, S. K., and M. Lockwood (2006), A numerical model of the ionospheric signatures of time-varying magnetic reconnection: 3. Quasi-instantaneous convection responses in the Cowley-Lockwood paradigm, *Ann. Geophys.*, *24*, 961–972.

- Nicolls, M. J., and C. J. Heinselman (2007), Three-dimensional measurements of traveling ionospheric disturbances with the Poker Flat Incoherent Scatter Radar, *Geophys. Res. Lett.*, *34*, L21104, doi:10.1029/2007GL031506.
- Oksavik, K., J. M. Ruohoniemi, R. A. Greenwald, J. B. H. Baker, J. Moen, H. C. Carlson, T. K. Yeoman, and M. Lester (2006), Observations of isolated polar cap patches by the European Incoherent Scatter (EISCAT) Svalbard and Super Dual Auroral Radar Network (SuperDARN) Finland radars, *J. Geophys. Res.*, *111*, A05310, doi:10.1029/2005JA011400.
- Oksavik, K., V. L. Barth, J. Moen, and M. Lester (2010), On the entry and transit of high-density plasma across the polar cap, *J. Geophys. Res.*, *115*, A12308, doi:10.1029/2010JA015817.
- Pitout, F., and P. Blelly (2003), Electron density in the cusp ionosphere: Increase or depletion?, *Geophys. Res. Lett.*, *30*(14), 1726, doi:10.1029/2003GL017151.
- Pitout, F., C. P. Escoubet, and E. A. Lucek (2004), Ionospheric plasma density structures associated with magnetopause motion: A case study using the Cluster spacecraft and the EISCAT Svalbard Radar, *Ann. Geophys.*, *22*, 2369–2379.
- Rodger, A. S., M. Pinnock, J. R. Dudeney, K. B. Baker, and R. A. Greenwald (1994), A new mechanism for polar patch formation, *J. Geophys. Res.*, *99*, 6425–6436.
- Ruohoniemi, J., and K. Baker (1998), Large-scale imaging of high-latitude convection with SuperDARN HF radar observations, *J. Geophys. Res.*, *103*, 20,797–20,811.
- Schunk, R. W., W. J. Raitt, and P. M. Banks (1975), Effect of electric fields on the daytime high-latitude E and F regions, *J. Geophys. Res.*, *80*, 3121.
- Sojka, J. J., M. D. Bowline, R. W. Schunk, D. T. Decker, C. E. Valladares, R. Sheehan, D. N. Anderson, and R. A. Heelis (1993), Modeling polar cap F-region patches using time varying convection, *Geophys. Res. Lett.*, *20*, 1783–1786, doi:10.1029/93GL01347.
- Sojka, J. J., M. J. Nicolls, C. J. Heinselman, and J. D. Kelly (2009), The PFISR IPY observations of ionospheric climate and weather, *J. Atmos. Sol. Terr. Phys.*, *71*, 771–785, doi:10.1016/j.jastp.2009.01.001.
- Stolle, C., J. Liliensten, S. Schlüter, C. Jacobi, M. Rietveld, and H. Lühr (2006), Observing the north polar ionosphere on 30 October 2003 by GPS, imaging and IS radars, *Ann. Geophys.*, *24*, 107–113, doi:10.5194/angeo-24-107-2006.
- Thomas, E. G., J. B. H. Baker, J. M. Ruohoniemi, L. B. N. Clausen, A. J. Coster, J. C. Foster, and P. J. Erickson (2013), Direct observations of the role of convection electric field in the formation of a polar tongue of ionization from storm enhanced density, *J. Geophys. Res. Space Physics*, *118*, 1180–1189, doi:10.1002/jgra.50116.
- Valladares, C. E., D. Alcaydè, J. V. Rodriguez, J. M. Ruohoniemi, and A. P. Van Eyken (1999), Observations of plasma density structures in association with the passage of traveling convection vortices and the occurrence of large plasma jets, *Ann. Geophys.*, *17*(8), 1020–1039, doi:10.1007/s00585-999-1020-6.
- Valladares, C., S. Basu, J. Buchau, and E. Friis-Christensen (1994), Experimental evidence for the formation and entry of patches into the polar cap, *Radio Sci.*, *29*, 167–194, doi:10.1029/93RS01579.
- Wang, H., and H. Lühr (2011), The efficiency of mechanisms driving Subauroral Polarization Streams (SAPS), *Ann. Geophys.*, *29*, 1277–1286, doi:10.5194/angeo-29-1277-2011.
- Wang, Z., J. K. Shi, K. Torkar, G. J. Wang, and X. Wang (2015), A case study on ionospheric scintillations at low latitude associated with a plasma blob observed in situ, *Geophys. Res. Lett.*, *42*, 2109–2114, doi:10.1002/2015GL063493.
- Wood, A. G., S. E. Pryse, and J. Moen (2009), Modulation of nightside polar patches by substorm activity, *Ann. Geophys.*, *27*, 3923–3932, doi:10.5194/angeo-27-3923-2009.
- Zhang, Q.-H., et al. (2011), On the importance of interplanetary magnetic field |By| on polar cap patch formation, *J. Geophys. Res.*, *116*, A05308, doi:10.1029/2010JA016287.
- Zhang, Q.-H., B.-C. Zhang, J. Moen, M. Lockwood, I. McCrea, H.-G. Yang, H.-Q. Hu, R.-Y. Liu, S.-R. Zhang, and M. Lester (2013a), Polar cap patch segmentation of the tongue of ionization in the morning convection cell, *Geophys. Res. Lett.*, *40*, 2918–2922, doi:10.1002/grl.50616.
- Zhang, Q.-H., et al. (2013b), Direct observations of the evolution of polar cap ionization patches, *Science*, *339*, 1597–1600, doi:10.1126/science.1231487.
- Zhang, Q.-H., M. Lockwood, J. C. Foster, S.-R. Zhang, B.-C. Zhang, I. W. McCrea, J. Moen, M. Lester, and J. M. Ruohoniemi (2015), Direct observations of the full Dungey convection cycle in the polar ionosphere for southward interplanetary magnetic field conditions, *J. Geophys. Res. Space Physics*, *120*, 4519–4530, doi:10.1002/2015JA021172.
- Zou, S., A. J. Ridley, M. B. Moldwin, M. J. Nicolls, A. J. Coster, E. G. Thomas, and J. M. Ruohoniemi (2013), Multi-instrument observations of SED during 24–25 October 2011 storm: Implications for SED formation processes, *J. Geophys. Res. Space Physics*, *118*, 7798–7809, doi:10.1002/2013JA018860.